ADVANCED FUNCTIONAL MATERIALS
www.afm-journal.de

Materials Views
www.MaterialsViews.com

The Impact of Carrier Transport Confinement on the Energy Transfer Between InGaN/GaN Quantum-Well Nanorods and Colloidal Nanocrystals

Bin Jiang, Chunfeng Zhang, Xiaoyong Wang, Min Joo Park, Joon Seop Kwak,* Jian Xu, Huichao Zhang, Jiayu Zhang, Fei Xue, and Min Xiao**

The energy transfer (ET) between InGaN/GaN multiple-quantum-well (MQW) nanorods (NRs) and semiconductor nanocrystals (NCs) for efficient color conversion is studied. An exceptional contribution of carrier transport confinement to the ET mechanisms is observed in the proximal side-wall coupling system, which consists of InGaN/GaN NRs and CdSe NCs. Under relatively low or high excitation, the ET rate shows different carrier-density dependence, resulting from different electron-hole configurations, i.e., bound excitons and free carriers. In the localized exciton regime, the ET rate decreases when increasing temperature from 20 K to 200 K. However, in the free-carrier regime, the ET rate varies insignificantly in the same temperature range. The temperature dependence in this NR-NC coupling system is different from that in the previously studied planar MQW-NC coupling system. It is suggested that the carrier transport confinement in NRs is a major factor for these divergences. The highly efficient ET with efficiency up to 80% shows a promising potential of using such NR-NC coupled structures for ET-pumped, NC-based, light-emitting devices.

1. Introduction

Energy transfer (ET) pumping of semiconductor nanocrystals (NCs) using InGaN/GaN heterostructures has recently been proposed as a method of color conversion for solid-state lighting.[1,2] In comparison to the conventional absorption-based approaches for color conversion, the nonradiative ET pumping can eliminate energy losses associated with the intermediate steps (including blue light emission, light extraction and re-absorption),[1] and it can circumvent the difficulty of current injection in the conventional NC-based p-n junction diodes.[3–8] The ET-pumped, NC-based light-emitting diodes (LEDs) have been demonstrated with improved performances in brightness, conversion efficiency, and color quality.[2,9–14] However, only very thin conductive layer can be used in the planar LED design in order to achieve close proximity between quantum-wells (QWs) and NCs.[2] Recently, nanostructured QWs with dry-etched nanopillar[15,16] or nanohole structures[17] have been introduced to incorporate the commonly used multiple-QW (MQW) structures with thick capping layers. With the side-wall coupling, highly efficient ET is realizable, revealing promises for LED optimization with nano-architectures.

The mechanisms underlying the ET between InGaN/GaN heterostructures and NCs are under intensive study in recent years. It is generally accepted that the ET is Förster type originating from the Coulomb interactions. The configuration and localization of carriers are reported to be the major factors governing the ET process.[18,19] A theoritical examination made by Kos et al. pointed out different aspects of the ET process

B. Jiang, Prof. C. Zhang, Prof. X. Wang, F. Xue
National Laboratory of Solid State Microstructures
and Department of Physics
Nanjing University
Nanjing 210093, China
E-mail: cfzhang@nju.edu.cn
M. J. Park, Prof. J. S. Kwak
Department of Printed Electronic Engineering
Sunchon National University
Sunchon, Jeonnam 540-742, Korea
E-mail: jskwak@sunchon.ac.kr
Prof. J. Xu
Department of Engineering Science and Mechanics
Penn State University
University Park, PA 16802, USA
H. Zhang, Prof. J. Zhang
Advanced Photonic Center
Southeast University
Nanjing 210096, China
Prof. M. Xiao
National Laboratory of Solid State Microstructures
and Department of Physics
Nanjing University
Nanjing 210093, China
E-mail: mxiao@uark.edu
Prof. M. Xiao
Department of Physics
University of Arkansas
Fayetteville, AR 72701, USA

DOI: 10.1002/adfm.201200351

when photo-induced carriers in QWs are configured in the form of bounded excitons or free carriers.[18] This work was in good agreement with the experimental results on a planar QW sample with high density defects studied by Achermann et al.[1,18] A recent experiment carried out by Rohrmoser et al.[19] reported the impact of exciton localization to the ET process in a planar QW-NC coupled structure. They observed an increase of ET rate when increasing temperature from 20 K to 150 K and attributed this temperature dependence to the reduction in the degree of carrier localization.[19] The mechanisms for the ET process in a side-wall coupling nanostructure may be different from that in a planar QW-NC structure, since nanofabrication could significantly influence the configurations and dynamics of the photo-induced carriers, owing to the reversal quantum-confined Stark effect (QCSE),[20–22] the carrier transport confinement,[23–25] and other effects.[26,27]

To clarify the impact of nanofabrication on the ET process, we carry out a systematic study on the proximal side-wall coupling system with InGaN/GaN MQW nanorod (NR)–NC structures. We find an exceptional contribution of carrier transport confinement to the ET process. Time-resolved photoluminescence (TRPL) spectra are recorded to quantitatively analyze the carrier-density-dependent ET rate. When the carrier density increases, the ET rate increases slowly under low power excitation but increases dramatically under high power excitation. The temperature dependence of the ET process is also different between the sample with low and high density carriers. When temperature goes up from 20 K to 200 K, the ET rate drops dramatically with low density but varies insignificantly with high density. The abnormal carrier-density dependence is probably due to the difference of carrier configuration, as most of photo-induced carriers are in the form of bounded excitons (free carriers) with low (high) carrier density at low (high) temperature. The temperature dependence in the hybrid NR-NC structure is different from the previously-studied planar MQW-NC coupled structure,[19] which can be attributed to the confinement of carrier transport as evidenced by the transient spectral data.

2. Results and Discussion

The proximal side-wall coupling is realized in a hybrid InGaN/GaN MQW NR-NC structure, with the fabrication process for MQW NRs shown in Figure S1 (Supporting Information). **Figure 1**a,b compares the TEM images of the planar MQWs and the MQW NRs. Each of the dry-etched NRs is configured with a MQW-embedded p-i-n heterojunction. NC phosphors are infiltrated into the spaces between these nanorods. The procedures are described in the Experimental Section. The five pairs of InGaN QWs are exposed to the sides after nanofabrication which can be proximally coupled to NCs by drop-coating (Figure 1c). For individual nanorod, the interaction with NCs induces ET as shown in the diagram of Figure 1e. We present a sideview of the whole hybrid structure in Figure S1g (Supporting Information), which can be directly used for LED demonstration after electrode deposition.

The emission band of the MQW NRs lies in the strong absorption region of the NCs (Figure 1d), providing a strong coupling between the NR excitations and the absorption dipoles of the NCs. Figure 1f displays a diagram of energy

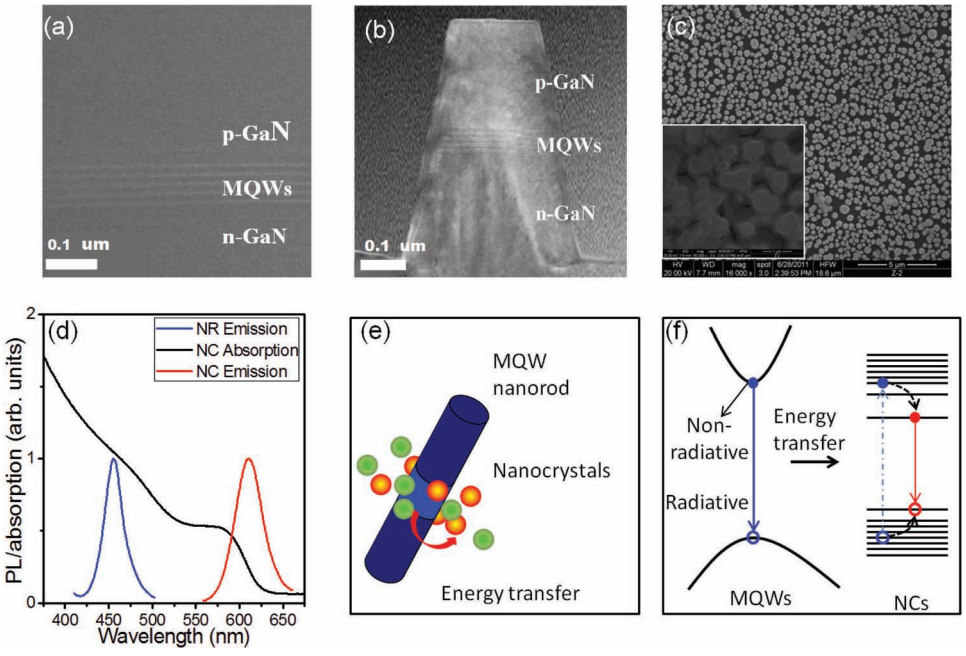

Figure 1. Morphologies and steady emission properties of the samples used in the study. TEM images of the parent planar InGaN/GaN MQWs (a) and a single NR (b). c) SEM images (top view) of the NR and hybrid NR-NC samples (inset). d) The emission spectrum of NRs is shown in comparison with the absorption/emission spectra of NCs. e) Diagram of the ET process between a single MQW NR and proximally coated NCs. f) Schematic diagram of energy levels involved in energy transfer from the MQW NRs to the NCs.

levels involved in the ET process.[1] After carrier thermalization and cooling, the photo-induced carriers in pure NRs can decay either radiatively or nonraditively. In the hybrid structure, carriers can recombine through the ET process. Hot carriers generated in the NCs by ET will experience fast intraband relaxation. Eventually, emission with photon energy of NC bandgap is generated primarily through interband transition in the NCs. With the presence of ET, the recombination rate of carriers increases from $\Gamma_R + \Gamma_{NR}$ to $\Gamma_R + \Gamma_{NR} + \Gamma_{ET}$, where Γ_R, Γ_{NR}, and Γ_{ET} are the rate of radiative recombination, nonratiave recombination and ET, respectively. Thus, the ET rate and efficiency can be analyzed by monitoring temporal evolution of PL emission from the NRs.

Temporal evolution of PL emission from the samples used here is different from the mono-exponential decay as observed in the planar QW samples with high density defects.[1,18] Similar to many previous reports on nitride emitters,[28–32] we record highly nonexponential TRPL decay traces in the MQW NRs. We employ a phenomenological stretched exponential (SE) function to interpret the experimental results.[30] Normalized TRPL curves can be well-described by a SE function in the form of $I(t) = \exp[-(t/\tau_0)^{\beta}]$, where τ_0 is the SE decay lifetime, and β expresses the rate distribution with the value between 0 (broad distribution) and 1 (narrow distribution). The presence of ET process is evidenced by having a shorter SE decay lifetime in the hybrid NR-NC samples than that in the pure NRs. However, it is inappropriate to directly regard the SE decay rate as the ET rate, since it is different from the average decay rate of the emitters.[33] We can evaluate the ET process with two parameters, i.e. integrated quantum efficiency (QE) and early-stage QE (their rigorous definitions are available in the Experimental Section) estimated by the dynamics over the whole and the first 250 picoseconds time windows, respectively.

Comparisons of the emission intensities as a function of delay time and emission wavelength recorded from the MQW NR samples and hybrid NR-NC samples at room temperature are presented in **Figure 2**a,b, respectively. The decay rate dramatically increases in the hybrid structure, serving as a signature of efficient ET. This increase of PL decay rate covers the whole emission band, indicating an efficient coupling between the donors and acceptors. The early-stage rate of ET (Γ_e) is measured by comparing different recombination rates at the early stage between pure NR and hybrid NR-NC samples. The value of Γ_e is critically dependent on the carrier densities (Figure 2c). The early-stage ET rate increases slowly with the carrier density below a density value of about 3×10^{12} cm^{-2}; Above this value, the slope of the density dependence is significantly increased. With the same excitation density, the integrated QE is lower than the early-stage QE, since the ET process is more efficient in the higher carrier density regime. Over 80% of ET efficiency at the early stage is observed with the carrier density close to 10^{13} cm^{-2}. Since the early-stage ET represents the conversion efficiency with continuous device operation, the high efficiency is promising for effective color conversion in such hybrid NR-NC coupling structures.

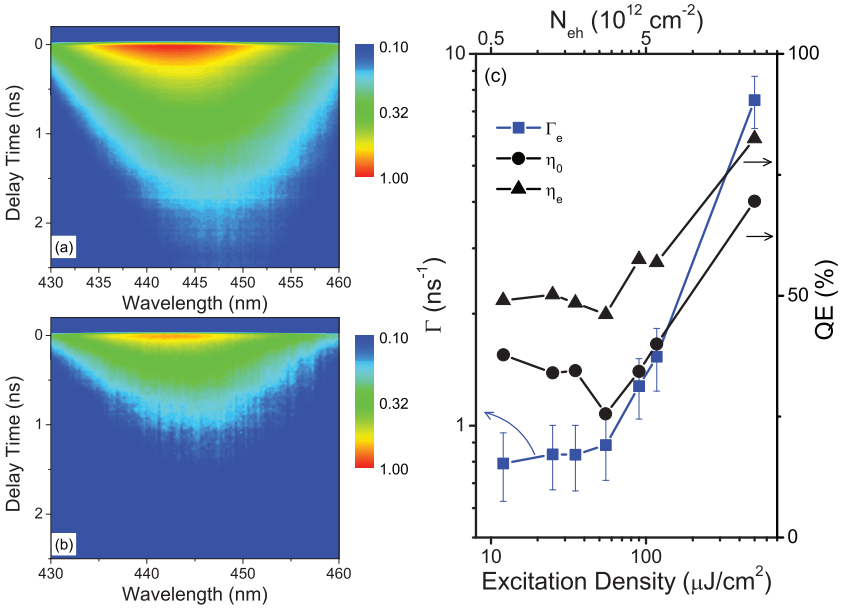

Figure 2. Characterization of ET process at room temperature. Transient emission intensity is plotted as a function of emission wavelength and delay time for pure NR (a) and hybrid NR-NC (b) samples. c) Early-stage ET rate, early-stage QE (η_e), and integrated QE (η_0) are plotted as a function of carrier density.

The temperature-dependent ET behaviors are different for samples with low and high power excitations. The TRPL traces of the pure NR and hybrid NR-NC samples are compared at various temperatures with excitation densities of 25 μJ/cm^2 (**Figure 3**a–d) and 500 μJ/cm^2 (Figure 3e–h). Carrier recombination in the samples is sensitive to the temperature, since the nonradiative decay rate increases with temperature. The estimated early-stage ET rates with relatively low and high power excitations, plotted as a function of temperature, are shown in **Figure 4**a and 4b, respectively. The temperature-dependent traces with different power excitations show significant divergence. With a relatively low excitation power, the ET rate dramatically decreases when increasing temperature from 20 K to 200 K; however, the ET rate varies insignificantly within the same temperature range when the excitation power is high.

To understand the experimental results described above, we first analyze the carrier configurations in the MQW NRs. When a QW sample is excited with low carrier density or is placed at low temperature, the photo-induced carriers stay in the form of bounded excitons. However, the configuration of free carriers will dominate when the temperature is sufficiently high to overcome the binding energy and/or the carrier density exceeds the value of a_B^{-2} (~10^{13} cm^{-2}, a_B is the exciton Bohr radius).[18,34] Most likely, the power-dependent ET rate shown in Figure 2c is a result of carrier configuration divergence. With high carrier density, free carriers contribute to the ET rate with a propotional power-dependence. With low carrier density, the ET rate varies insignificantly with excitation power where the bounded excitons may be dominant. This attribution is further examined

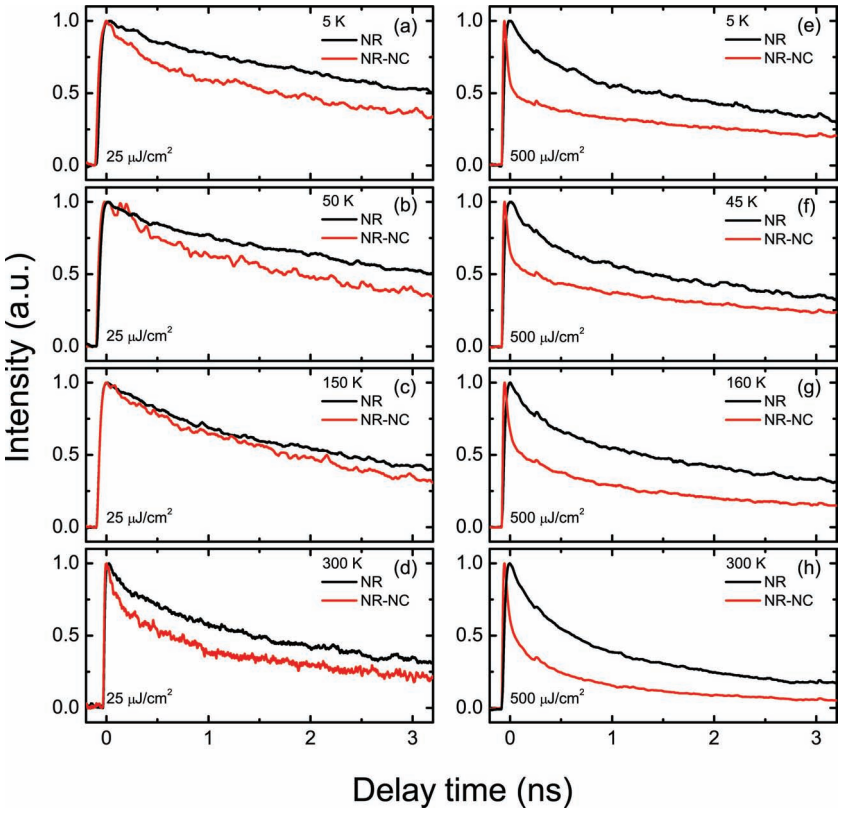

Figure 3. Temperature-dependent ET characterization. TRPL traces of pure NR and hybrid NR-NC samples with excitations at 25 μJ/cm² (a–d) and 500 μJ/cm² (e–h).

by carrier dynamics in the NRs at different temperatures. From the temperature-dependent TRPL traces, the parameters fitted to the SE function are plotted as a function of temperature in **Figure 5**a,b. At low temperature, the SE lifetime is much longer under a low power excitation with the distribution factor β close to 1, indicating a major role played by the bounded excitons. The contribution of free carriers becomes more and more important with an increase of the temperature and/or carrier density.

The degree of carrier localization can also affect the ET between MQW NRs and NCs. To obtain information of the carrier localization, we check the early-stage recombination rate (inset of Figure 5a) of carriers in the MQW NRs. The recombination lifetime decreases rapidly when the power increases to about 30 μJ/cm², but saturates to a value for further increase of the excitation power. This "saturation" effect has been explained by the reversal QCSE, or known as the free carrier screening effect.[21,22,32] The QCSE, caused by the strain-induced internal electric field, slows down the recombination of photo-induced carriers.[21,22,35,36] The reversal effect is the screening of internal electrical field by high density photo-induced free carriers. This effect is of more importance in NRs since the nanofabrication can partially relax the strain.[26,27] The free carriers can compensate the internal field more efficiently with lower density in MQW NRs. Since a lower degree of carrier localization is beneficial for the ET,[19] more efficient ET process can be achieved with a lower carrier density in the MQW NR-NC structure than in the planar structure, which may lead to the power dependence of the ET rate out of the propotional relation at low carrier density (Figure 2c).

Besides the configuration and localization of carriers, other factors should also be considered to fully understand the temperature-dependent results (Figure 4) in this study. With increasing temperature from 20 K to 200 K, the abnormal drop of the early-stage ET rate with low-power excitation cannot be explained by the carrier configuration or localization discussed above. With increasing temperature, the increased thermal energy would reduce the degree of carrier localization in QWs,[19] so an increase in ET rate is anticipated. This argument has been confirmed by the study on the planar QW-NC structure where ET rate increases with temperature in the range of 20 K – 150 K.[19] Apparently, the experimental data in this study (Figure 4a) in the hybrid NR-NC structure show a drop of ET rate with increasing temperature from 20 K to 200 K. One possible reason is due to the impact of nanofabrication on the carrier transport in MQW NRs. The average diameter of NRs is close to or even shorter than the carrier diffusion length in InGaN/GaN QWs,[37–39] so the boundaries of NRs can modify the intra-well carrier transport

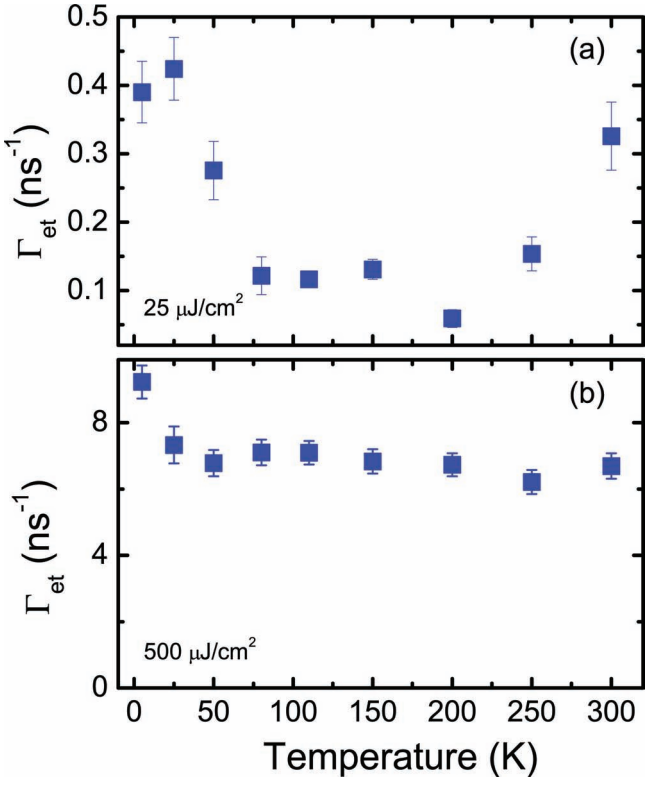

Figure 4. Temperature-dependent ET rate with excitations at 25 μJ/cm² (a) and 500 μJ/cm² (b).

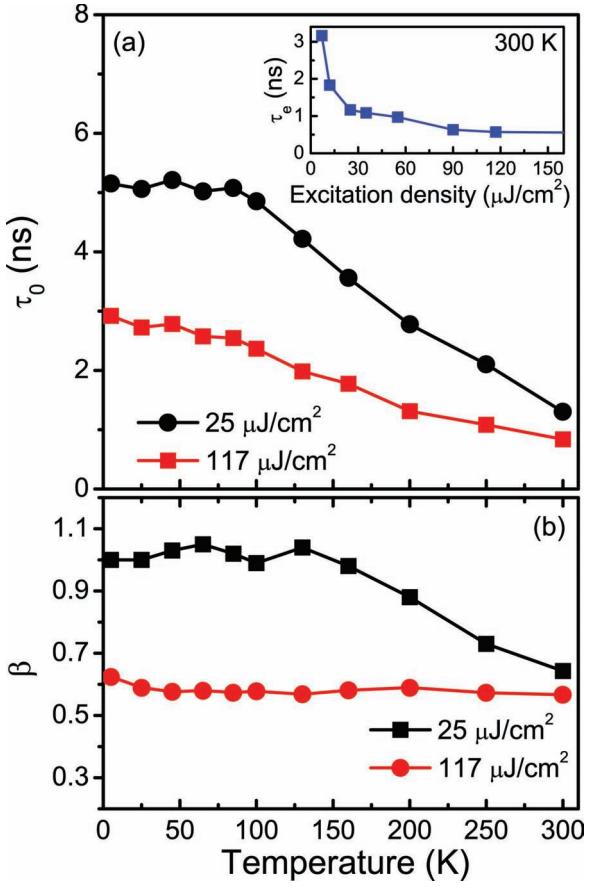

Figure 5. Carrier dynamics of InGaN/GaN MQW NRs. The best fitting SE parameters (SE decay lifetime and rate distribution) for TRPL traces at different temperatures with excitations at 25 μJ/cm^2 and 117 μJ/cm^2. Inset of (a) shows the early-stage recombination lifetime versus excitation density.

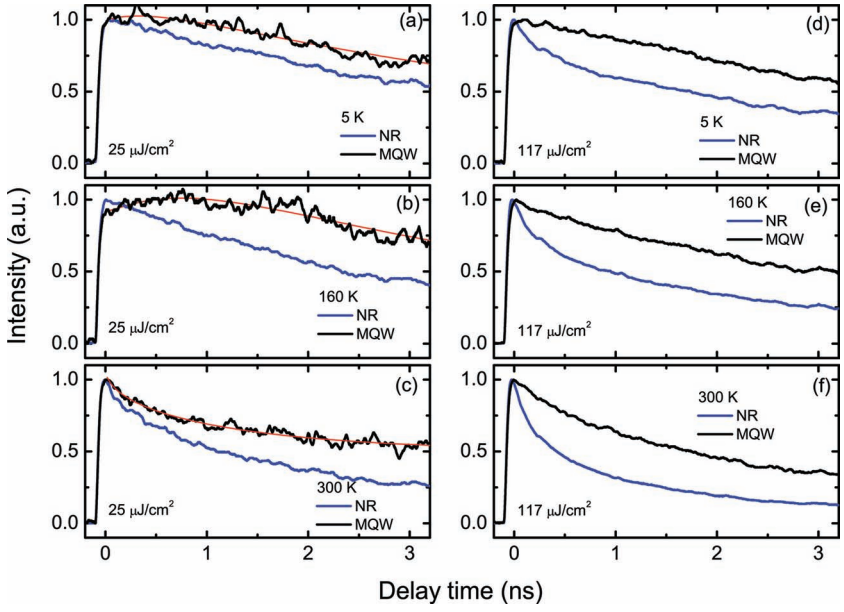

Figure 6. TRPL traces recorded at various temperatures in the NRs and the planar MQWs with excitations at 25 μJ/cm^2 and 117μJ/cm^2.

significantly.[25] We have checked the effect of carrier transport confinement in the NRs with the TRPL data. As shown in **Figure 6**a,b, the thermally activated carrier transport exhibits a delayed rise in the TRPL traces in the parent planar MQWs, but such delayed rise is absent in the TRPL traces recorded for the NRs. When increasing temperature, the weakly-localized carriers close to the boundary may couple to the strongly-localized states in the center of NRs, leading to a relatively weak ET process. As a consequence, the rate drop of ET process with temperature is observed in the hybrid NR-NC structure with low carrier density (Figure 4a). When the excitation power is high, most of the carriers are "free" and the confinement of carrier transport become less important. Despite of a slight difference in the recombination lifetime, the temperature dependence of TRPL follows a similar trend in both planar MQW and MQW NR samples (Figures 6d–f). Hence, the ET rate varies insignificantly in the temperature range of 20–200 K (Figure 4b).

From above discussions, one can conclude that multiple mechanisms may be involved in the ET process between the InGaN/GaN MQW NRs and NCs. Although carrier configuration and localization influence the ET in the side-wall coupling system similar to that in the planar coupling structures, the impact of carrier transport confinement on the ET is only present in the hybrid NR-NC structure. These effects are the major factors that induce the abnormal power and temperature dependences of the ET rate in the hybrid NR-NC structure.

3. Conclusions

In this study, we investigate the mechanisms of ET from InGaN MQW NRs to side-wall coupled NCs with TRPL spectroscopy. Different carrier configurations contribute to the ET process in hybrid NR-NC structures as revealed in the power-dependent meaurements. The free carriers dominate in the high carrier density regime at room temperature, while the bounded excitons contribute more in the low density regime at low temperature. The effects of carrier transport confinement and carrier screening can have impacts on the ET rate. These experimental results suggest that the ET process can be optimized with high current injection in LED devices. The highly efficient ET (>80%) from NR to NCs makes the hybrid design an excellent candidate for color conversion, which significantly improves charge injection into the NC emitters. Considering the highly efficient light extraction in NR LEDs,[40–43] the nano-architectures studied in this work will be helpful for the hybrid nitride-NC system to find applications in next-generation optoelectronic devices.

4. Experimental Section

Sample Preparation: The MQWs on sapphire substrates consist of a GaN buffer, an n-type GaN layer, five pairs of 2.5 nm-thick $In_{0.1}Ga_{0.9}N$ QWs

sandwiched between 13 nm GaN barriers, a p-type of GaN layer, as well as a p-type capping layer. A schematic diagram of the nanofabrication procedure is available in the Supporting Information (Figure S1, Supporting Information). The InGaN/GaN MQW NRs with an average diameter of 200 nm are fabricated from an InGaN/GaN epitaxial MQW LED structure by inductively-coupled-plasma etching using a novel etch mask of self-assembled ITO-based nanodots,[44] which is described as follows: a SiO_2 layer was first deposited on the top surface of the LED wafer by plasma-enhanced chemical vapor deposition (PECVD) (Figure S1b, Supporting Information), and an indium tin oxide (ITO) layer was subsequently deposited onto the SiO_2 layer with electron beam evaporation (Figure S1c,Supporting Information). The as-deposited ITO film can be assumed to be an oxygen-poor ITO layer, which has a mixture of metallic phase and ITO phase, since the ITO films were deposited by using electron beam evaporator. Next, the sample was dipped into 3% HCl solution to dissolve the ITO phase, which left self-assembled ITO-based nanodots on the SiO_2 layer (Figure S1d, Supporting Information). The SiO_2 layer was then patterned with a fluorine-based dry-etching process using the ITO-based nanodots as the etch mask (Figure S1e, Supporting Information). Finally, the InGaN/GaN NR heterostructure was formed by dry-etching the LED wafer via the patterned SiO_2 hard mask (Figure S1f, Supporting Information). By controlling the size of the ITO-based nanodots and the ICP etching conditions, NRs with diameters ~200 nm and ~50% filling factor were fabricated successfully. An etching depth of ~0.6 μm was designed to reach the n-type layer of the LED heterojunction and to laterally expose the emissive quantum wells along the sidewall of the NRs. Finally the sidewall surface of the NRs is conformally coated with QD phosphors.

The trioctylphosphineoxide (TOPO) capped CdSe NCs (~10 mg/mL) in toluene were synthesized by the hot-injection organometallic route as previously described.[45] The mixture of 20 g trioctylphosphine oxide and 0.25 g cadmium acetate dihydrate was heated to 300 degree under Ar ambience and then injected with the Se precursor (the mixture of 0.4 g Se and 10 ml trioctylphosphine), and the sizes of CdSe NCs were controlled by the reaction time. These CdSe NCs were purified before they were drop-cast onto the NRs, and the purification process was done by precipitating NCs with methanol and acetone, and then dissolving them in toluene.

Optical Characterization: Second harmonic light (400 nm) of optical pulses generated from a Ti:Sapphire regenerative amplifier (800 nm wavelength, 90 fs pulse duration, 1 kHz repetation rate, Libra, Coherent Inc) is used to excite the InGaN QW layers only. The samples are excited from the backside to keep the carrier density same in pure NR and hybrid NR-NC samples. Carrier density is changed with excitation flux in the range of 7-500 $\mu J/cm^2$ (corresponding to carrier density between 2×10^{10} and 1.2×10^{13} cm^{-2} in single wells). Time-integrated emission spectra are measured with a fiber spectrometer (USB 2000+, Ocean-Optics). The technique of optical Kerr gating is utilized to perform TRPL studies with the Kerr medium of a 5 mm thick carbon sulfide cell. The temporal resolution is about 2 ps. The PMT (5784-20, Hamamatsu) is used to record the TRPL traces with a band-pass optical filter centered at 450 nm with 40 nm bandwidth. The emission spectra at different decay times are recorded with a 0.5 meter spectrometer (SP 2500i, Princeton Instruments) attached a liquid-nitrogen-cooled CCD. A liquid helium cryostat (MicrocCryostatHe, Oxford) is used to perform temperature-dependent measurements from 5 K to 300 K.

Data Analysis: The SE function is only a phenomenological model for the TRPL traces. The SE decay rate differs from the average rate especially when the distribution is broad. The recovery of rate distributions in the case of SE decay is very difficult mathematically, but one can quantitively evaluate the ET with two unambiguous parameters (i.e., integrated QE and early-stage QE). The integrated QE, defined as $\eta_0 = 1 - E_{DA}/E_D$ (E_D and E_{DA} are the total emission energies in the NR and hybrid NR-NC samples, respectively), can be approximately calculated with the equation

$$\eta_0 = 1 - \frac{\int_0^\infty e^{-(t/\tau_{ow})^{\beta w}} dt}{\int_0^\infty e^{-(t/\tau_{owo})^{\beta wo}} dt},$$

where w and wo denote the measurements done in hybrid samples with NCs and NR samples without NCs, respectively. η_0 integrates the ET process over time post-excitation that includes the carrier-density-dependent radiative and nonradiative relaxations. This integrated QE is a vital value describing ET efficiency with pulse-induced carriers in most optical studies. In electrically-driven LEDs, the carrier density and relaxation rate remain stable over time. The ET rate in the devices can be approximately estimated with the early-stage carrier dynamics from optical experimental data with the same carrier density. The fast decay component at the early stage (i.e. the first 250 ps) of the temporal decay window in InGaN/GaN heterostructures follows an exponential decay well.[31] The ET rate can then be calculated as the difference between two early-stage relaxation rates, i.e., $\Gamma_e = 1/\tau_e = 1/\tau_{ew} - 1/\tau_{ewo}$, where τ_{ew} and τ_{ewo} are the early-stage relaxation times in the MQW NRs with and without NCs, respectively. The early-stage QE of ET can be estimated as $\eta_e = 1 - \tau_{ew}/\tau_{ewo}$. An example of the data analysis is available in Supporting Information.

Supporting Information

Supporting Information is available from the Wiley Online Library or from the author.

Acknowledgements

This work is supported by the Program of International S&T Cooperation (2011DFA01400, MOST), the National Basic Research Program of China (2012CB921801, 2011CBA00205), National Science Foundation of China (61108001, and 11021403), NRF of Korea grant funded by the Korea government (MEST) (K2011-0017325). C.Z. acknowledges financial support from New Century Excellent Talents program (NCET-09-0467) and Fundamental Research Funds for the Central Universities (1107020420, 1118020406, 1104020403, and 1115020404). J.S.K acknowledges financial support from WCU program in SCNU.

Received: February 6, 2012
Revised: April 10, 2012
Published online: May 3, 2012

[1] M. Achermann, M. A. Petruska, S. Kos, D. L. Smith, D. D. Koleske, V. I. Klimov, *Nature* **2004**, *429*, 642.
[2] M. Achermann, M. A. Petruska, D. D. Koleske, M. H. Crawdord, V. I. Klimov, *Nano Lett.* **2006**, *6*, 1396.
[3] T.-H. Kim, K.-S. Cho, E. K. Lee, S. J. Lee, J. Chae, J. W. Kim, D. H. Kim, J.-Y. Kwon, G. Amaratunga, S. Y. Lee, B. L. Choi, Y. Kuk, J. M. Kim, K. Kim, *Nat. Photonics* **2011**,*5*, 176.
[4] V. L. Colvin, M. C. Schlamp, A. P. Alivisatos, *Nature* **1994**, *370*, 354.
[5] J. M. Caruge, J. E. Halpert, V. Wood, V. Bulovic, M. G. Bawendi, *Nat. Photonics* **2008**, *2*, 247.
[6] Q. J. Sun, Y. A. Wang, L. S. Li, D. Y. Wang, T. Zhu, J. Xu, C. H. Yang, Y. F. Li, *Nat. Photonics* **2007**, *1*, 717.
[7] K. -S. Cho, E. K. Lee, W. J. Joo, E. Jang, T.-H. Kim, S. J. Lee, S.-J. Kwon, J. Y. Han, B.-K. Kim, B. L. Choi, J. M. Kim, *Nat. Photonics* **2009**, *3*, 341.
[8] Q. J. Sun, G. Subramanyam, L. M. Dai, M. Check, A. Campbell, R. Naik, J. Grote, Y. Wang, *ACS Nano* **2009**, *3*, 737.
[9] S. Nizamoglu, T. Erdem, X. W. Sun, H. V. Demir, *Opt. Lett.* **2010**, *35*, 3372.
[10] S. Nizamoglu, G. Zengin, H. V. Demir, *Appl. Phys. Lett.* **2008**, *92*, 031102.
[11] S. Nizamoglu, H. V. Demir, *Opt. Express* **2008**, *16*, 13961.
[12] S. Nizamoglu, E. Sari, J.-H. Baek, I. -H. Lee, H. V. Demir, *New J. Phys.* **2008**, *10*, 123001.

[13] S. Nizamoglu, E. Mutlugun, T. Özel, H. V. Demir, S. Sapra, N. Gaponik, A. Eychmüller, *Appl. Phys. Lett.* **2008**, *92*, 113110.
[14] E. J. Park, T. Erdem, V. Ibrahimova, S. Nizamoglu, H. V. Demir, D. Tuncel, *ACS Nano,* **2011**, *5*, 2483.
[15] F. Zhang, C. Zhang, J. Xu, M. J. Park, J. S. Kwak, S. E. Mohney, presented at CLEO/QELS **2010**, San Jose, CA
[16] S. Nizamoglu, B. Guzelturk, D.-W. Jeon, I. -H. Lee, H. V. Demir, *Appl. Phys. Lett.* **2011**, *98*, 163108.
[17] S. Chanyawadee, P. G. Lagoudakis, R. T. Harley, M. D. B. Charlton, D. V. Talapin, H. W. Huang, C.-H. Lin, *Adv. Mater.* **2010**, *22*, 602.
[18] Š. Kos, M. Achermann, V. I. Klimov, D. L. Smith, *Phys. Rev. B* **2005**, *71*, 205309.
[19] S. Rohrmoser, J. Baldauf, R. T. Harley, P. G. Lagoudakis, S. Sapra, A. Eychmüller, I. M. Watson, *Appl. Phys. Lett.* **2007**, *91*, 092126.
[20] G. Sun, G. Xu, Y. J. Ding, H. Zhao, G. Liu, J. Zhang, N. Tansu, *Appl. Phys. Lett.* **2011**, **99**, 081104.
[21] T. Kuroda, A. Tackeuchi, T. Sota, *Appl. Phys. Lett.* **2000**, *76*, 3753.
[22] T. Kuroda, A. Tackeuchi, *J. Appl. Phys.* **2002**, *92*, 3071.
[23] S.-W. Feng, Y.-C. Cheng, Y.-Y. Chung, C. C. Yang, M. -H. Mao, Y.-S. Lin, K.-J. Ma, J.-I. Chyi, *Appl. Phys. Lett.* **2002**, *80*, 4375.
[24] S. -W. Feng, Y.-C. Cheng, Y.-Y. Chung, C. C. Yang, Y.-S. Lin, C. Hsu, K.-J. Ma, J.-I. Chyi, *J. Appl. Phys.* **2002**, *92*, 4441.
[25] B. Jiang, C. Zhang, X. Wang, F. Xue, M. J. Park, J. S. Kwak, M. Xiao, arXiv:1111.4010.
[26] Y. R. Wu, C. H. Chiu, C. Y. Chang, P. C. Yu, H. C. Kuo, *IEEE J. Sel. Topics. Quantum Electron.* **2009**, *15*, 1226.
[27] V. Ramesh, A. Kikuchi, K. Kishino, M. Funato, Y. Kawakami, *J. Appl. Phys.* **2010**, *107*, 114303.
[28] A. Morel, P. Lefebvre, S. Kalliakos, T. Taliercio, T. Bretagnon, B. Gil, *Phys. Rev. B* **2003**, *68*, 045331.
[29] I. L. Krestnikov, N. N. Ledentsov, A. Hoffmann, D. Bimberg, A. V. Sakharov, W. V. Lundin, A. F. Tsatsul'nikov, A. S. Usikov, Z. I. Alferov, Y. G. Musikhin, D. Gerthsen, *Phys. Rev. B* **2002**, *66*, 155310.
[30] T. Bartel, M. Dworzak, M. Strassburg, A. Hoffmann, A. Strittmatter, D. Bimberg, *Appl. Phys. Lett.* **2004**, *85*, 1946.
[31] C. N. Brosseau, M. Perrin, C. Silva, R. Leonelli, *Phys. Rev. B* **2010**, *82*, 085305.
[32] P. Lefebvre, S. Kalliakos, T. Bretagnon, P. Valvin, T. Taliercio, B. Gil, N. Grandjean, J. Massies, *Phys. Rev. B* **2004**, *69*, 035307.
[33] A. F. Van Driel, I. S. Nikolaev, P. Vergeer, P. Lodahl, D. Vanmaekelbergh, W. L. Vos, *Phys. Rev. B* **2007**, *75*, 035329.
[34] C. F. Klingshirn, *High Excitation Effects and Nonlinear Optics, Semiconductor Optics*, Springer-Verlag, Berlin Heidelberg **2007**, p. 467.
[35] S. M. de Sousa Pereira, K. P. O'Donnell, E. J. da Costa Alves, *Adv. Funct. Mater.* **2007**, *17*, 37.
[36] T. Takeuchi, S. Sota, M. Katsuragawa, M. Komori, H. Takeuchi, H. Amano, I. Akasaki, *Jpn. J. Appl. Phys.* **1997**, *36*, L382.
[37] V. Liuolia, S. Marcinkevičius, Y.-D. Lin, H. Ohta, S. P. DenBaars, S. Nakamura, *J. Appl. Phys.* **2010**, *108*, 023101.
[38] S. Chichibu, K. Wada, S. Nakamura, *Appl. Phys. Lett.* **1997**, *71*, 2346.
[39] J. Danhof, U. T. Schwarz, A. Kaneta, Y. Kawakami, *Phys. Rev. B* **2011**, *84*, 035324.
[40] C. Hahn, Z. Zhang, A. Fu, C. H. Wu, Y. J. Hwang, D. J. Gargas, P. Yang, *ACS Nano* **2011**, *5*, 3970.
[41] W. Guo, M. Zhang, A. Banerjee, P. Bhattacharya, *Nano Lett.* **2010**, *10*, 3355.
[42] H. M. Kim, Y. H. Cho, H. Lee, S. II. Kim, S. R. Ryu, D. Y. Kim, T. W. Kang, K. S. Chung, *Nano Lett.* **2004**, *4*, 1059.
[43] K. S. Kim, S. M. Kim, H. Jeong, M. S. Jeong, G. Y. Jung, *Adv. Funct. Mater.* **2010**, *20*, 1076.
[44] C. H. Chiu, T. C. Lu, H. W. Huang, C. F. Lai, C. C. Kao, J. T. Chu, C. C. Yu, H. C. Kuo, S. C. Wang, C. F. Lin, T. H. Hsueh, *Nanotechnology* **2007**, *18*, 445201.
[45] J. Aldana, Y. A. Wang, X. G. Peng, *J. Am. Chem. Soc.* **2001**, *123*, 8844.